Research Article

Roger Gómez-Herrera[#], Paula Alfonso-Triguero[#], Xiaoman Mao, Juan Mancebo-Aracil, David Montpeyó, Fernando Novio, Julia Lorenzo^{*}, and Daniel Ruiz-Molina^{*}

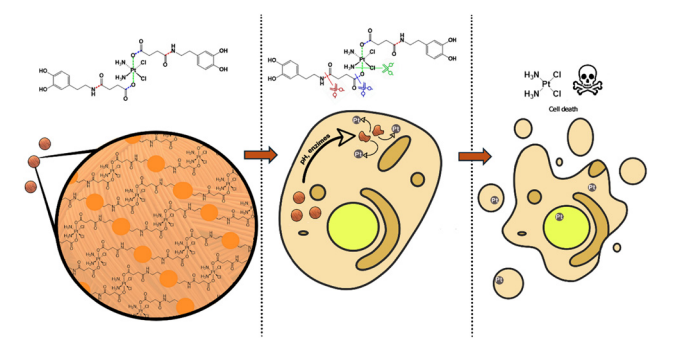
Bioinspired neuromelanin-like Pt(IV) polymeric nanoparticles for cancer treatment

https://doi.org/10.1515/ntrev-2024-0118 received December 21, 2023; accepted October 23, 2024

Abstract: To expand the chemotherapeutic potential of platinum complexes, different approaches have been followed, two of the most relevant being their administration as the prodrug Pt(iv) and encapsulation in nanocarriers. Herein, we demonstrate how neuromelanin may become a good bioinspiration for the synthesis of nanoparticles (NPs), combining both approaches. For this, complex PtBC reacts with sodium periodate, inducing a melanization process and the formation of nanoparticles. *In vitro* results on nonmalignant human fibroblast cells (1Br3G), human cervical

Paula Alfonso-Triguero: Catalan Institute of Nanoscience and Nanotechnology (ICN2), CSIC and BIST, Campus UAB, Bellaterra, 08193, Barcelona, Spain; Institut de Biotecnologia i Biomedicina, and Departament de Bioquímica i Biologia Molecular, Universitat Autònoma de Barcelona, Cerdanyola del Vallès, 08193, Barcelona, Spain Juan Mancebo-Aracil: Instituto de Química del Sur (INQUI-SUR-CONICET) – NANOSYN, Departamento de Química, Universidad Nacional del Sur (UNS), Av. Alem 1253, 8000, Bahía Blanca, Buenos Aires, Argentina

David Montpeyó: Institut de Biotecnologia i Biomedicina, and Departament de Bioquímica i Biologia Molecular, Universitat Autònoma de Barcelona, Cerdanyola del Vallès, 08193, Barcelona, Spain Fernando Novio: Departament de Química, Universitat Autònoma de Barcelona (UAB), Campus UAB, Cerdanyola del Vallès, 08193, Barcelona, Spain



Graphical abstract

cancer, murine glioma (GL261), and human ovarian cancer confirmed its therapeutic efficacy. The role of the Pt(IV) ion on the cytotoxicity effects was confirmed by comparison with the results obtained for a family of nanoparticles obtained with nordihydroguaiaretic acid under the same experimental conditions. Finally, intranasal administration of the NPs in orthotopic glioblastoma multiforme murine models in female C57BL/6 mice showed excellent *in vivo* biodistribution and tolerability. Overall, this innovative approach represents a step toward more specific and less toxic therapies in the field of cancer chemotherapy.

Keywords: chemotherapy, polyphenol, melanin, polydopamine, cancer cells

1 Introduction

The serendipitous discovery of the antitumor effectiveness of cisplatin (CDDP) in the late 1960s [1–5] marked a crucial moment in cancer chemotherapy [6–8]. Since then, platinum (Pt)-based anticancer drugs have shown well-defined mechanisms of action and significant therapeutic effects, making them widely used in clinical settings. However, despite their evident efficacy, especially against ovarian tumors, Pt(II) complexes are non-specific chemotherapeutic drugs that induce systemic toxicity [9–12]. To mitigate secondary effects, various strategies have been employed. The first approach involves the use of Pt(IV) produgs, which have

[#] These authors contributed equally to this work and should be considered first co-authors.

^{*} Corresponding author: Julia Lorenzo, Institut de Biotecnologia i Biomedicina, and Departament de Bioquímica i Biologia Molecular, Universitat Autònoma de Barcelona, Cerdanyola del Vallès, 08193, Barcelona, Spain; Centro de Investigación Biomédica en Red: Bioingeniería, Biomateriales y Nanomedicina, 08193, Cerdanyola del Vallès, Spain, e-mail: Julia.lorenzo@uab.cat

^{*} Corresponding author: Daniel Ruiz-Molina, Catalan Institute of Nanoscience and Nanotechnology (ICN2), CSIC and BIST, Campus UAB, Bellaterra, 08193, Barcelona, Spain, e-mail: dani.ruiz@icn2.cat Roger Gómez-Herrera, Xiaoman Mao: Catalan Institute of Nanoscience and Nanotechnology (ICN2), CSIC and BIST, Campus UAB, Bellaterra, 08193, Barcelona, Spain

an octahedral geometry. As a result, Pt(IV) complexes are less susceptible to ligand substitution and only reduced to the active Pt(II) form upon tumor cell internalization, reducing toxicity and secondary administration adverse effects [13-17]. The second strategy involves the use of nanoformulations [18-23]. Owing to their small size and large surface area, nanoparticles enhance both drug bioavailability and permeability retention in tumor tissues [24]. Additionally, nanoparticles can transport and increase the solubility of various therapeutic agents, protect them from degradation and mononuclear phagocyte action, enable targeted release, and allow for real-time in vivo monitoring as well as combined anticancer therapies [25-34]. Accordingly, Pt-based nanoformulations have significantly reduced toxicity and improved drug delivery to tumors, with a concomitant increase in survival rates [35]. However, despite these pioneering successful results, the use of nanoparticles is still at an incipient stage, with the need for more studies to be developed.

The use of bioinspired approaches in searching for new and innovative solutions to cancer treatment has represented a step forward [36]. Of special interest has been polydopamine in its nanoparticulated state [37,38]. In this context, inspired by neuromelanin particles found in dopaminergic neurons of the substantia nigra, we recently reported the bis-catechol functionalized Pt(IV) prodrug complex PtBC (Scheme 1) and its use to form coordination polymeric nanoparticles (Pt-Fe NCPs) because of the affinity of catechol units to chelate iron metal ions [39]. In vivo intranasal administration of Pt-Fe NCPs in orthotopic preclinical GL261 glioblastoma (GB) multiforme tumorbearing mice showed enhanced platinum tumor accumulation and prolonged survival of the tested cohort, in some cases even to complete cure [40]. These successful initial findings encouraged us to investigate alternative possibilities to optimize the chemotherapeutic effect of this novel family of nanoparticles. One potential approach involves polymerization of PtBC through a

bioinspired melanization process by reaction with sodium periodate, without the need for iron metals [41,42]. In addition to ensure more robust nanoparticles and controlled platinum release, with this approach, we aim to significantly increase the platinum encapsulation efficiency. A schematic representation for the synthesis of the novel nanoparticles (referred to from now on as pPtBC NPs) is shown in Scheme 1.

The in vitro therapeutic efficacy of pPtBC NPs in nonmalignant human fibroblast cells (1Br3G), human cervical cancer (HeLa), murine glioma (GL261), and human ovarian cancer showed excellent results. This efficiency was unequivocally attributed to the presence of Pt(IV) ions. This comparison was made with the toxicity results obtained for a related family of nanoparticles obtained under the same experimental conditions but replacing PtBC with bis-catechol nordihydroguaiaretic acid (NDGA). NDGA is a polyphenol with well-described antitumoral capabilities and structurally comparable to that of PtBC; elongated with a sterically bulky center and ending catechol groups, but lacking the Pt core. On top of that, in vivo biodistribution and tolerability of pPtBC NPs have also been thoroughly evaluated via intranasal administration using orthotopic GB murine models.

2 Materials and methods

2.1 Materials

Solvents and starting materials were acquired from Sigma-Aldrich (Madrid, Spain) and employed in their original state without additional purification unless otherwise specified. PtBC was synthesized following the methodology reported earlier [39].



Scheme 1: Schematic protocol for the synthesis of polymeric pPtBC NPs, by reaction of PtBC with sodium periodate (see section 2.3 for more details). For comparison purposes, related nanoparticles were obtained with the same methodology but NDGA as ligand, exhibiting a related topology to that of PtBC, but lacking the Pt(Iv) ion.

2.2 Characterization methods

The size distribution and surface charge of the nanoparticles (0.5 mg/mL) were measured by dynamic light scattering (DLS) using a ZetasizerNano 3600 instrument (Malvern Instruments, UK), with a size range limit from 0.6 to 6 nm. Scanning electron microscopy (SEM) images were obtained using a SEM (FEI Quanta 650 FEG) at an acceleration voltage of 5-20 kV. SEM samples were prepared by drop-casting the corresponding dispersions of nanoparticles (NPs) on aluminum tape followed by solvent evaporation under room conditions. Before analysis, the samples were metalized with a thin layer of platinum (thickness of 5 nm) using a sputter coater (Emitech K550). NPs size from SEM imaging was obtained using analytical software Image [(Copyright (C) 1989, 1991 Free Software Foundation, Inc.) using the integrated particle analysis software from binary file images taken from 8-bit format files from SEM imaging. Fourier transform infrared (FT-IR) spectra were recorded using a Tensor 27 spectrometer (Bruker Optik GmbH, Germany) with HBr pellets. Inductively coupled plasma mass spectrometry (ICP-MS) (PerkinElmer Inc. Germany) measurements were recorded using ¹⁹⁴Pt, ¹⁹⁵Pt, and ¹⁹⁶Pt as Pt tracers.

2.3 Synthesis of pPtBC NPs and pNDGA NPs

Synthesis of pPtBC NPs. PtBC (10.0 mg, 0.013 mmol) was dissolved in 6 mL of a 1:1 mixture of ethanol:MilliQ water. Sodium periodate (5.3 mg, 0.024 mmol) was dissolved in 0.4 mL of MilliQ water. The sodium periodate solution was then added dropwise to the PtBC solution and heated to 30°C. Addition was carried out with a syringe pump, and addition was carried over a period of 1 h (6.7 µL/min) under vigorous stirring (1,500 rpm). The reaction was then allowed to evolve for 3 h at 30°C in the dark. The product was then isolated by centrifugation (10 min at 12,000 rpm), washed multiple times with ethanol and water, and resuspended in water for storing, yielding pPtBC NPs as a brown turbid suspension in a 3.0 mg yield (for more information, see Supporting Information S1).

Synthesis of pNDGA NPs. NDGA (20.0 mg, 0.066 mmol) was dissolved in 28 mL of a 1:1 mixture of ethanol:MilliO water. Sodium periodate (28.2 mg, 0.132 mmol) was dissolved in 4 mL of MilliQ water. The sodium periodate solution was then added dropwise to the NDGA solution. Addition was carried out with a syringe pump, and addition was carried over a period of 1h (66.7 µL/min) under vigorous stirring (1,500 rpm). The reaction was then allowed to evolve for 3 h in the dark. The product was then isolated by centrifugation (10 min at 12,000 rpm), washed multiple times with ethanol and water, and resuspended in water for storing, yielding 4.5 mg of the pNDGA NPs as a brown turbid suspension (for more information, see Supporting Information S3).

2.4 Drug release assay

Drug release from pPtBC NPs was evaluated using the dialysis method. Concentrated pPtBC NPs (1 mg/mL) were reconstituted in 1 mL of Milli-O water and placed in dialysis bags (MWCO = 6,000-8,000 Da, where MWCO stands for Molecular Weight Cut-Off). The bags were then immersed in sealed beakers containing 40 mL of PB buffer with pH values set at 7.4 and 5.5. The beakers were then kept at 37°C with gentle stirring throughout the study. At predetermined time points, a 500 mL aliquot was withdrawn from the dialysate and immediately replaced with an equal volume of fresh buffer. The quantity of released Pt was determined using ICP-MS.

2.5 Cell lines culture

Cell lines, including the human cervical cancer cell line HeLa, non-malignant human fibroblast cell line 1Br3G, murine GB cell line GL261, and a pair of human ovarian cancer cell lines, A2780 and its cisplatin-resistant counterpart A2780/cis, were obtained from the American Type Culture Collection (ATCC; Manassas, Virginia, USA 30-4,500 K). Specifically, HeLa cells were cultured in minimal essential medium (MEM), 1Br3G in Dulbecco's modified eagle medium (DMEM), GL261 and A2780 in Roswell park memorial institute medium 1640 (RPMI 1640), and A2780/cis in RPMI 1640 supplemented with 1 µM of cisplatin. All culture media were enriched with 10% fetal bovine serum (FBS; Gibco®, Invitrogen, UK), 0.285 g/L glutamine, 2.0 g/L sodium bicarbonate, and 1% penicillin-streptomycin. The cells were grown as adherent monolayers and maintained in an incubator (HERAcell, 150i, Thermo Scientific) at 37°C in 5% CO₂ with a relative humidity of 95%, except for 1Br3G, which was maintained at 10% CO₂. All cell culture media, FBS, supplements, antibiotics, trypsin, and Trypan Blue were procured from Fisher Scientific (Gibco[®], Invitrogen, UK).

2.6 *In vitro* cytotoxicity assays

Cells (HeLa, 1Br3G, GL261, A2780, and A2780/cis) in the exponential growth phase were seeded into a 96-well plate (Corning, USA) under optimal conditions. Each cell type was seeded at specific densities: HeLa at 2,000 cells/well, 1Br3G at 3,000 cells/well, GL261 at 4,000 cells/well, and both A2780 and A2780/cis at 3,000 cells/well. Specifically, cisplatin-containing cell culture media were replaced with fresh RPMI media without the drug 4h before seeding. After 24 h of incubation, fresh media containing compounds (pPtBC NPs, PtBC, and cisplatin [CDDP]) at various concentrations (0, 0.1, 1, 5, 10, 25, 50, 100, 200 µM referred to Pt concentration) were added, and the plates were incubated for either 24 or 72 h. Subsequently, 10 µL of PrestoBlue[®] (0.15 mg/mL, Thermo Scientific, USA) was added to each well. The plates were then further incubated for 4 h before measuring the fluorescence at 572 nm with excitation at 531 nm using the microplate reader Victor 3 (Perkin Elmer, USA). For 1Br3G, the incubation time with PrestoBlue[®] was extended to 7 h to ensure a sufficient difference in fluorescence intensity between concentrations. All experiments were conducted in triplicate, and the data were analyzed using Graphpad Prism (version 7.0). The calculated IC₅₀s were obtained by Graphpad Prism.

2.7 Estimation of reactive oxygen species (ROS) formation

HeLa, 1Br3G, and GL261 cells were seeded in black 96-well plates (Corning, USA) at a density of 20,000 cells at each well to ensure full confluence. Following a 24-h incubation, the spent medium was removed, and the cells were rinsed with serum-free medium. Subsequently, pre-warmed PBS containing the fluorescent probe 2',7'-dichlorofluorescin diacetate (DCFCDA) at a final working concentration of 10 mM was added, and the cells were incubated for 30 min. Once the probe was internalized, the buffer containing the probe was replaced with either medium alone or media-containing compounds (H₂O₂, pPtBC NPs, pNDGA NPs, PtBC, NDGA, and CDDP) at the IC₅₀ concentration for 24 h. A positive control with 0.1 mM H₂O₂ was included for comparison. After 24 h, the fluorescence of each well was measured at 530 nm with excitation at 485 nm using a microplate reader (Victor 3, Perkin Elmer, USA). This experiment was independently repeated in triplicate, and the results were normalized based on the negative control, which was loaded with the dye but lacked drug treatment.

2.8 Cellular internalization studies

HeLa, 1Br3G, and GL261 cells were seeded in six-well plates (Corning, USA) at a density of 300,000 cells at each well

with 1.5 mL of media. Following a 24-h incubation, the old media were replaced with 1 mL of fresh media with or without CDDP, PtBC, and pPtBC NPs at a concentration of 0.1 mM referred to as Pt. The treated cells were allowed to internalize the compounds for 6 and 24 h at the incubator. Another cellular uptake assay was conducted with a reduced concentration of Pt (10 μ M) and extended time points of 2, 4, 8, and 24 h. The media were promptly removed, and the cells were washed twice with cold PBS to eliminate excess compounds. Subsequently, 0.5 mL of trypsin was added to each well for 3 min, and a twofold volume of fresh media was added to neutralize the trypsin. After taking an aliquot from each well for cell counting, the remaining cell suspensions were collected into 1.5 mL Eppendorf tubes (Corning, USA) and centrifuged at 12,000 rpm for 4 min. The supernatants were discarded, and the cell pellets were stored at -80°C for further quantification by ICP-MS.

DE GRUYTER

2.9 DNA-bound Pt

To elucidate the mechanism of action of our PtBc NPs, we conducted DNA extraction and quantification using ICP-MS to measure the DNA-bound Pt after a 24-h uptake in HeLa, 1Br3G, and GL261 cells. Cells in exponential growth phase were seeded onto cell culture dishes under optimal conditions for each cell line, reaching 50–60% confluence within 24 h before treatment. Subsequently, CDDP, PtBC, and pPtBC NPs were added at a concentration of 0.1 mM referred to Pt, and the cells were allowed to incubate for an additional 24 h. Following this incubation period, media containing drugs were removed, and the cells were washed, trypsinized, collected by centrifugation, and rinsed twice with cold PBS to eliminate excess drugs.

The resulting cell pellets were resuspended in lysis buffer (pH 8.0, 150 mM Tris-HCl, 100 mM NaCl, and 0.5% [w/v] SDS). The pellets in the buffer were incubated on ice for 15 min and then centrifuged at 15,000 rpm for 15 min. To each supernatant, 0.1 volume of RNase A was added at 0.2 mg/mL and incubated for 1h at 37°C. Subsequently, Proteinase K was added at 0.1 mg/mL and incubated for 3 h at 56°C. A volume of phenol/chloroform/isoamyl alcohol (25:24:1 in volume, Thermo Scientific®) was added and mixed gently. After centrifugation of 3 min at 15,000 rpm, aqueous phases containing DNA were transferred into sterile tubes. DNA was precipitated with 0.1 volume of 3 M sodium acetate and 1 volume of absolute ethanol at -20°C overnight. Then, the DNA samples were centrifuged for 15 min at 15,000 rpm, and finally, DNA samples were dried and resuspended in 0.1 mL of elution buffer (pH 8.0, 10 mM Tris-HCl, 1 mM EDTA, ethylenediaminetetraacetic acid). The concentration of isolated DNA was quantified by measuring the absorbance at 260 nm using a NanoDropTM 1,000 spectrophotometer (Thermo Fisher Scientific, USA). The remaining samples were frozen for ICP-MS analysis.

2.10 Sample digestion treatments for ICP-MS measurement

For ICP-MS preparation, all glassware underwent a 48-h immersion in 20% HNO₃, whereas plasticware was soaked in 5% HNO₃ for 4 h prior to use. The samples were digested using a wet digestion method, with procedures tailored to specific materials.

2.10.1 Chemical samples

The precise amount of the sample was weighed using an analytical balance and transferred to a vial. Concentrated ultrapure HNO₃ (69%, Ultratrace[®], ppb-trace analysis grade, Scharlab, Spain) was then added. The samples were left in a fume hood for 48 h for complete digestion, then diluted with 0.5% (v/v) ultrapure HNO₃ for subsequent measurements.

2.10.2 Cell pellets

Cell pellets were resuspended in approximately 100 mL of concentrated ultrapure HNO₃ (69%, Ultratrace[®], ppb-trace analysis grade, Scharlab, Spain) and left to digest overnight. The samples were heated to 90°C until the suspensions became clear. Subsequently, the samples were diluted with 0.5% (v/v) ultrapure HNO₃ to appropriate volumes for later measurements.

2.10.3 Tissues

Tissues were combined with T-PERTM buffer (Thermo Fisher Scientific, USA) at a ratio of 10 mL/g, then cut into small pieces and subjected to sonication using an ultrasonication microtip (Branson Digital Sonifier 450, Emerson, USA) over repetitive cycles of 10 s active and 15 s inactive with an amplitude of 40%. The tissue suspensions were then added with aqua regia (all ppb-trace analysis grade) and heated up to 300°C, with 30% H₂O₂ added in the later digestion process until the suspensions became clear. The clear solutions were then transferred and diluted with 0.5% (v/v) ultrapure HNO₃ to appropriate volumes for the determination of metal contents using ICP-MS.

2.11 Animal studies

Animal experiments and care were conducted in collaboration with duly accredited personnel. Healthy female C57BL/ 6] mice aged 8-12 weeks, with a body weights ranging from 20 to 24 g, were used for in vivo investigations. The mice were procured from Charles River Laboratories (Charles River Laboratories Internacional, L'Abresle, France) and were accommodated in the Universitat Autònoma de Barcelona's animal facility (Servei d'Estabulari, https://estabulari.uab.cat/; accessed on 24 March 2022). Ethical approval for all animal study protocols was obtained from the local ethics committee (Comissió d'Ètica en l'Experimentació Animal i Humana, https://www.uab.cat/etica-recerca/; accessed on 24 March 2022), following regional and state legislation (protocol CEEAH-4859). The animals were kept in cages with unrestricted access to standard food and water, maintaining consistent housing and environmentally controlled conditions.

2.12 Preclinical model generation and treatment administration

Tumors were induced *via* intracranial stereotactic injection of 10⁵ GL261 glioma cells in the caudate nucleus. To facilitate intranasal administration, the animals were anesthetized with isoflurane for a minute and positioned in a supine orientation. Each nostril received a 2 µL dosage of the pPtBC NPs formulation, spaced with a 1-2 min interval between administrations. The well-being of treated animals was observed, and those exhibiting signs of distress were humanely euthanized in adherence to ethical considerations.

2.13 In vivo MRI studies

Mice bearing GL261 GB tumors underwent MRI scans for tracking alterations in tumor location and volume. The investigations were conducted using a 7T BioSpec 70/30 USR spectrometer (Bruker BioSpin GmbH) at the joint nuclear MR facility of UAB and CIBER-BBN, Unit 25 of NAN-BIOSIS. In brief, T2-weighted MRIs were acquired using a rapid acquisition with relaxation enhancement sequence. Key acquisition parameters included a repetition time (TR)/ effective echo time (TEeff) of 4,200/36 ms, echo train length of 8, field of view of 19.2 mm × 19.2 mm, matrix size of 256 × 256 (75 μ m/pixel × 75 μ m/pixel), 10 slices, slice thickness (ST) of 0.5 mm, inter-slice thickness (IT) of 0.1 mm, number of averages (NA) of 4, and a total acquisition time of 6 min

and 43 s. The collected MRI data underwent processing using ParaVision 5.1 software on a Linux platform.

To calculate tumor volume from the MRI acquisitions, ParaVision software delineated regions of interest (ROIs) to measure tumor area in each slice. Subsequently, mice tumor volumes were computed using the following formula:

$$TV(mm^3) = [(AS_1 \times ST) + [(AS_2 + (...) + AS_{10}) \times (ST + IT)]] \times 0.075^2.$$

Here, TV is the tumor volume, AS indicates the number of pixels within the ROI defined by tumor boundaries in each MRI slice, ST is the slice thickness (0.5 mm), IT is the interslice thickness (0.1 mm), and 0.075² signifies the individual pixel surface area in mm².

2.14 Tolerability assays

Healthy female C57BL/6 mice, aged 8-12 weeks and weighing 20–24 g, were randomly assigned to three groups: control, PtBC, and pPtBC NPs, with three mice in each group. The drugs were administered intranasally using a micropipette, while the mice were lightly anesthetized and positioned horizontally for the procedure. The dosage started at 0.9 mg Pt/kg body weight and gradually increased incrementally to 1.5 mg Pt/kg over 3 weeks, with doses administered weekly. Initial body weights were recorded, and subsequent monitoring occurred three times a week. Throughout the 4-week study, veterinary personnel closely monitored mice for mortality, food and water consumption, and suffering clinical signs. To assess tolerability in treated mice, we used statistical comparisons among groups utilizing a one-way analysis of variance followed by Bonferroni's multiple comparison test for three or more groups. A statistically significant P value was considered when less than 0.05.

2.15 In vivo biodistribution study

For the study, Pt NCPs were administered through intranasal delivery at a dosage of 1.5 mg Pt/kg body weight in GL261 GB-bearing mice. After 1 h, the mice were euthanized, and organs such as the brain, tumor, heart, lungs, spleen, liver, and kidneys were removed and weighed. These collected tissues underwent homogenization in T-PER buffer using an ultrasound probe with 30% amplitude and cycles of 10 s on and 15 s off. Next, the samples underwent centrifugation at 10,000 rpm for 10 min. A portion of each supernatant was extracted for total protein

quantification, while the remaining fraction was subjected to digestion following the previously outlined procedure. This prepared the samples for ICP-MS measurement, enabling the determination of Pt concentration.

2.16 Statistical analyses

Unless stated otherwise, values are given as the average plus or minus the standard error. A two-tailed Student's t-est for independent measurements was employed for making comparisons. Survival rate comparisons were conducted using the log-rank test. The significance threshold for all tests was set at p < 0.05, and values falling between 0.05 and 0.1 were regarded as a "trend toward significance."

3 Results and discussion

3.1 Synthesis and characterization

PtBC, obtained as previously described (for more information, see Supporting Information S1), was dissolved in a 1:1 ethanol:water solution and afterwards oxidized by slow and controlled addition of a NaIO₄ aqueous solution under vigorous stirring at 30°C to yield pPtBC NPs as spherical nanoparticles of 157 ± 0.5 nm and good homogeneity across all samples, as characterized by SEM imaging (Figure 1a). This size was in accordance with DLS, values, which exhibit a hydrodynamic size of 234.6 \pm 0.5 nm and a very low PDI of 0.087 ± 0.022 (C-potential was -37.1 ± 0.95 mV) (Figure 1c and d). FT-IR showed peaks in the 1,200–1,400 cm⁻¹ characteristic catechol region, though with a notable shift, the disappearance of the peaks at 1,283, 1,327, and 1,197 cm⁻¹ and the appearance of a new broad peak at 1,279 cm⁻¹ from oxidation products. Inductively coupled plasma optical emission spectrometry gave a platinum content value of 17%, slightly lower than the expected one of 24% for the theoretical formula; the decrease in Pt content w/w could be attributed to a nanoparticle weight increase due to the incorporation of sodium, and other ions present in the media, into the nanoparticle as a result of the oxidation process dopamine is undergoing (for more information, see Supporting Information S2).

pNDGA NPs were obtained following the same oxidative polymerization. SEM images showed the formation of spherical and homogeneous-shaped nanoparticles of 260 \pm 0.5 nm and good homogeneity across all samples. DLS

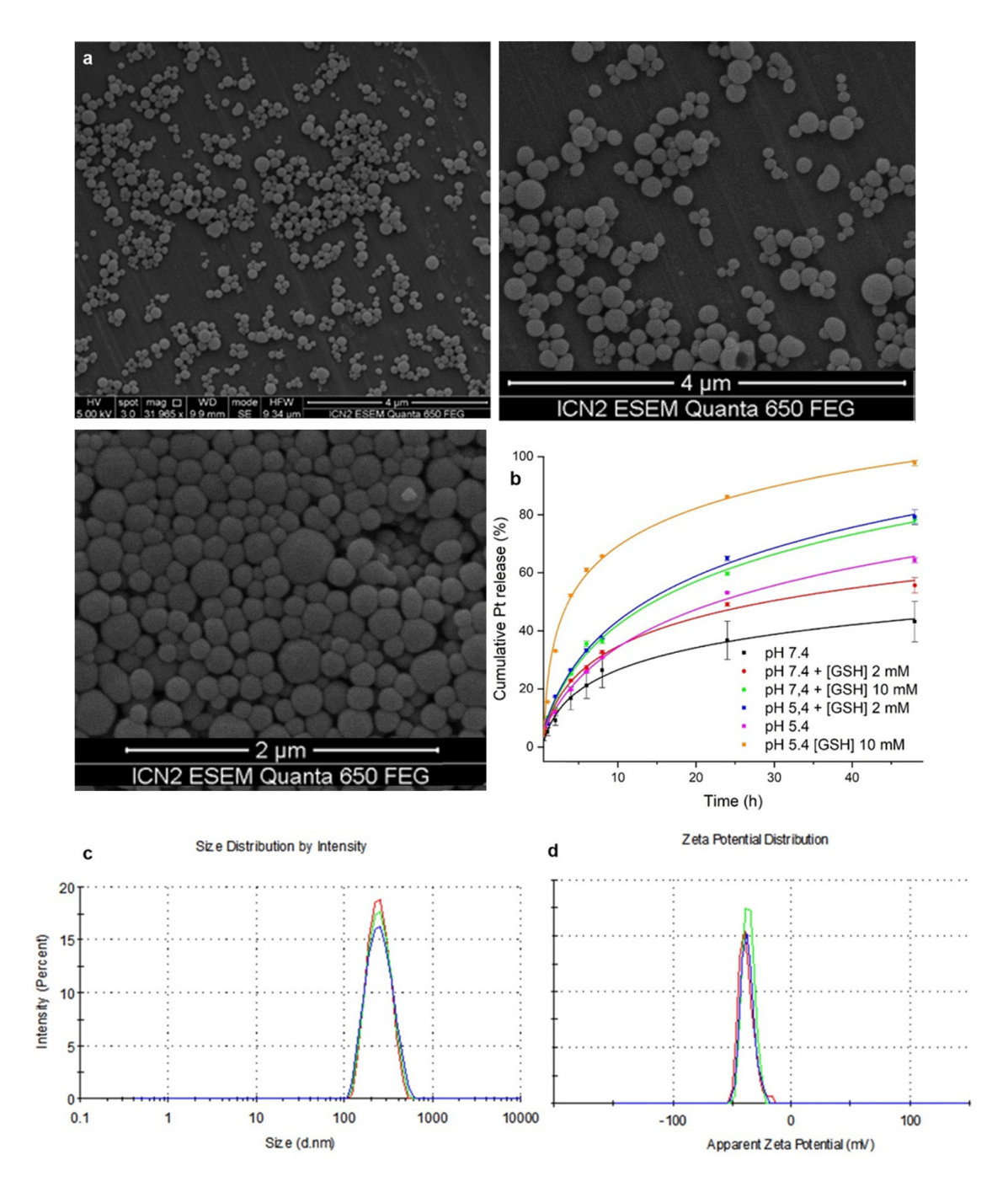


Figure 1: (a) Representative SEM images of pPtBC NPs under a 5 nm Pt thin film coating for imaging. (b) Cumulative Pt release from pPtBC NPs at pH 5.4 and 7.4 and in the presence of GSH (2 and 10 mM). (c) Representative size distribution by DLS. (d) Representative ζ-potential of pPtBC NPs by DLS.

experiments showed sizes of 214.2 ± 0.8 nm with a very low PDI of 0.07 \pm 0.02 and a ζ -potential of -28.7 ± 0.5 mV. FT-IR characterization showed a noticeable shift of the peaks characteristic of the catechol region (1,200–1,400 cm⁻¹), and once more the disappearance of peaks at 1,393, 1,354, 1,325, and 1,292 cm⁻¹ along with the appearance of new broad peaks at 1,279 and 1,725 cm⁻¹.

3.2 Platinum-controlled release

A dialysis methodology was used to obtain the 48-h platinum release profile of pPtBC NPs dispersed in a pH 7.4 phosphate buffer solution, mimicking in vitro physiological media, and a pH 5.5 environment simulating the lysosomal conditions [43]. The results, as quantified by ICP-MS, are shown in Figure 1b. In both scenarios, a typical release profile is observed with a disparity in release rates under acidic conditions. The release after 48 h at pH 7.4 and pH 5.5 was $43.20 \pm 6.92\%$ Pt and $64.34 \pm 0.9\%$, respectively.

Another important consideration is the reductive power, or redox homeostasis, of cells. Glutathione (GSH) and its oxidized form, glutathione disulfide, play pivotal roles in maintaining these redox capabilities within cells. In normal cells, their intracellular concentrations typically range from 1 to 10 mM, but in cancer cells, this concentration can increase up to fourfold [44]. To delve further into the influence of cellular redox state, we conducted the release profile experiments under varying GSH concentrations of 2 and 10 mM, while maintaining the same previous conditions. At pH 7.4 and 2 mM GSH, the measured Pt release was 55.7 \pm 2.63%, while it increased up to 78.23 ± 1.05% at 10 mM GSH. On the contrary, pH 5.4 and a 2 mM GSH concentration, the Pt release was already high, reaching 79.16 ± 2.53%, increasing up to 97.7 ± 0.92% at 10 mM. As observed, the combined effect of decreasing pH and the presence of GSH notably increases the release rates in these nanosystems.

3.3 Cytotoxicity effects

The *in vitro* cytotoxicity of PtBC and pPtBC NPs was evaluated and compared to cisplatin (CDDP) against a set of cancer cell lines: human cervical cancer cell line HeLa, the non-malignant human fibroblast cell line 1Br3G, murine glioma cell line GL261, the ovarian cancer cell line A2780, and the cisplatin-resistant counterpart cell line A2780/cis. It is worth noting that previous studies have shown that nanocarriers can bypass the efflux of resistant cells to free drug, leading to modulating or overcoming cancer cell resistance [45,46]. The assessments were conducted using the well-established PrestoBlue method, with data collected at both 24- and 72-h intervals. The half-maximal inhibitory concentrations (IC₅₀S) were calculated using

Graphpad Prism and are summarized in Table 1. At 24 h, PtBC and pPtBC NPs showed comparable cytotoxicity for HeLa and 1Br3G, while in the case of GL261 and A2780 cells, the IC_{50} value for PtBC is almost half of that found for pPtBC NPs. It is worth mentioning that IC_{50} values in both cases are comparable but slightly higher than those found for CDDP, except for ovarian A2780 cells where, interestingly, PtBC exhibits higher toxicity. After 72 h of exposure, the cytotoxicity difference between PtBC, pPtBC NPs, and CDDP diminished, approaching comparable IC_{50} values for Hela (even smaller for pPtBC NPs), GL261 cells, and A2780. In the case of 1Br3G and A2780/cis, both PtBC and pPtBC NPs exhibit similar values, but double those found for CDDP; even pathways for NPs uptake and detoxification are greatly influenced by the cell type [47].

The *in vitro* cytotoxicity of NDGA and pNDGA NPs was also tested for comparison purposes against the same panel of cancer cells (the results are shown in Table 2). As can be seen there, NDGA showed very low cytotoxicity in all the cell lines except for A2780 or A2780/cis, where surprisingly IC_{50} values are comparable and even smaller than CDDP. It is worth mentioning that pNDGA NPs were non-toxic in a given concentration range with cell viability close to 100% in all cell lines either for 24 or for 72 h.

3.4 ROS effects

Compounds containing catechol moieties, typically found in polyphenols and flavonoids, have been recognized for their diverse range of beneficial properties, including hepatoprotective, anti-inflammatory, antioxidant, and even anticancer effects [48]. However, it is worth noting that the oxidation of these catechol moieties can also lead to the generation of ROS, potentially resulting in excessive oxidative stress that could harm cells, leading to toxicity, damage, and inflammation [49]. Therefore, it is of particular interest to investigate ROS contribution to the cytotoxic properties of PtBC and

Table 1: IC₅₀s of CDDP, PtBC, and pPtBC NPs against a panel of cell lines

	Compounds	Cell lines						
		HeLa	1Br3G	GL261	A2780	A2780/cis		
24 h	CDDP	15.98 ± 1.04	45.07 ± 4.60	5.61 ± 0.28	13.95 ± 1.24	23.68 ± 1.74		
	PtBC	29.94 ± 1.04	56.09 ± 1.18	17.40 ± 1.08	10.98 ± 0.56	18.39 ± 1.85		
	pPtBC NPs	22.09 ± 1.09	56.30 ± 1.32	33.56 ± 1.36	18.44 ± 2.19	31.40 ± 2.28		
72 h	CDDP	2.34 ± 0.30	4.63 ± 0.42	2.16 ± 0.26	1.57 ± 0.08	5.22 ± 1.21		
	PtBC	1.85 ± 0.36	10.80 ± 0.60	4.17 ± 0.12	2.59 ± 0.33	9.12 ± 0.69		
	pPtBC NPs	0.65 ± 0.14	8.01 ± 0.72	4.64 ± 0.05	3.10 ± 0.32	10.50 ± 0.84		

pPtBC NPs, using the fluorescent probe 2',7'-DCFCDA in HeLa, 1Br3G, and GL261 cells [50]. After 24 h of exposure, strong DCF fluorescence was only observed in all the cells treated with NDGA and H₂O₂, the positive control. Neither PtBC nor the polymeric pPtBC/pNDGA NPs triggered the formation of ROS in any of the tested cell lines (Figure 2a-c). Notably, CDDP itself did not induce ROS generation.

3.5 Cellular uptake and DNA-bound Pt

The therapeutic efficacy of an anticancer agent greatly depends on its capacity to accumulate within the target, i.e. its intracellular concentration. This accumulation is directly related to several factors, including uptake pathways kinetics, metabolism, and/or cellular efflux. Increasing the lipophilicity of NPs' surface was also reported to increase the affinity to the cell membrane, including those of the blood-brain barrier (BBB), as opposed to hydrophilic NPs [51]. The polymeric nature of pPtBC NPs could potentially facilitate their transport, enhancing their cellular uptake within target tumor cells.

PtBC and pPtBC NPs (0.1 mM referred to as Pt) were coincubated with HeLa, 1Br3G, and GL261 cells for 6 h and afterwards digested and analyzed using ICP-MS. As depicted in Figure 2d, the cellular uptake exhibited the following trend PtBC > pPtBC NPs > CDDP. CDDP and PtBC are both small molecules that typically enter cells through passive diffusion, though cellular internalization for CDDP is dominated by the carriers present on the cell membrane, especially copper transporters and organic cation transporters [52,53]. The carrier-mediated endocytosis requires energy consumption, unlike passive diffusion, which might explain the lower cellular uptake of CDDP compared to PtBC. NPs commonly rely on endocytosis pathways, which are also energy dependent. With a relatively high extracellular concentration, PtBC potentially enters cells more easily than the NPs.

After a 24-h exposure (Figure 2e), the cellular uptake of these compounds remained relatively stable in HeLa cells,

suggesting a rapid internalization already after 6 h. However, in the other two cell lines, uptake levels continued to fluctuate even after 24 h. In 1Br3G cells, the intracellular level of CDDP was comparable to that of 6 h, while the levels of PtBC and pPtBC NPs decreased dramatically. However, they were still significantly higher than the CDDP level. Interestingly, the trend in GL261 cells inverted totally. The cellular uptake of CDDP increased 8.5 times in comparison to the intracellular concentration at 6 h, surpassing the levels of PtBC or pPtBC NPs.

Additional studies to determine DNA-bound platinum were also done by incubating CDDP, PtBC, and pPtBC NPs (100 µM) with HeLa, 1Br3G, and GL261 cells for 24 h. Then, nuclear DNA was extracted, purified, and quantified by absorbance; meanwhile, the amount of Pt bound to the DNA was quantified using ICP-MS. As illustrated in Figure 2f, the DNA-bound platinum concentration from intrinsically active CDDP was notably higher than that of PtBC and pPtBC NPs in all cell lines, indicating that not all Pt agents entering cells can effectively access the nucleus to bind to DNA. It is worth mentioning that PtBC and pPtBC NPs exhibited comparable anticancer activities over 24 h, suggesting that their cytotoxicity is not limited to Pt-DNA adducts. Increasing reports demonstrated that Pt agents can also bind to other cellular macromolecules such as RNA and proteins and may even induce immunogenic effects [54,55]. For instance, Bose et al. reported platinum complexes with high cytotoxicity like cisplatin, yet it exhibited no DNA binding at all [56].

3.6 In vivo tolerability and biodistribution via Intranasal administration

For these studies, we selected intranasal administration compared to other systemic routes, such as intravenous and intraperitoneal injections. Currently, there is a lack of reports detailing the biodistribution of Pt nanostructured agents through this pathway, even though it could hold significant value for future treatments.

Table 2: IC₅₀s of NDGA and pNDGA NPs against a panel of cell lines

	Compounds	Cell lines					
		HeLa	1Br3G	GL261	A2780	A2780/cis	
24 h	NDGA	164.15 ± 0.02	NT ^b	109.45 ± 1.95	8.94 ± 0.69	15.67 ± 2.14	
	pNDGA NPs	NT ^b					
72 h	NDGA	55.65 ± 6.21	14.20	81.73 ± 2.40	7.82 ± 0.39	12.96 ± 1.48	
	pNDGA NPs	NT ^b					

b NT represents non-toxic, meaning the viability of cells remains close to 100% even at the maximum concentration.

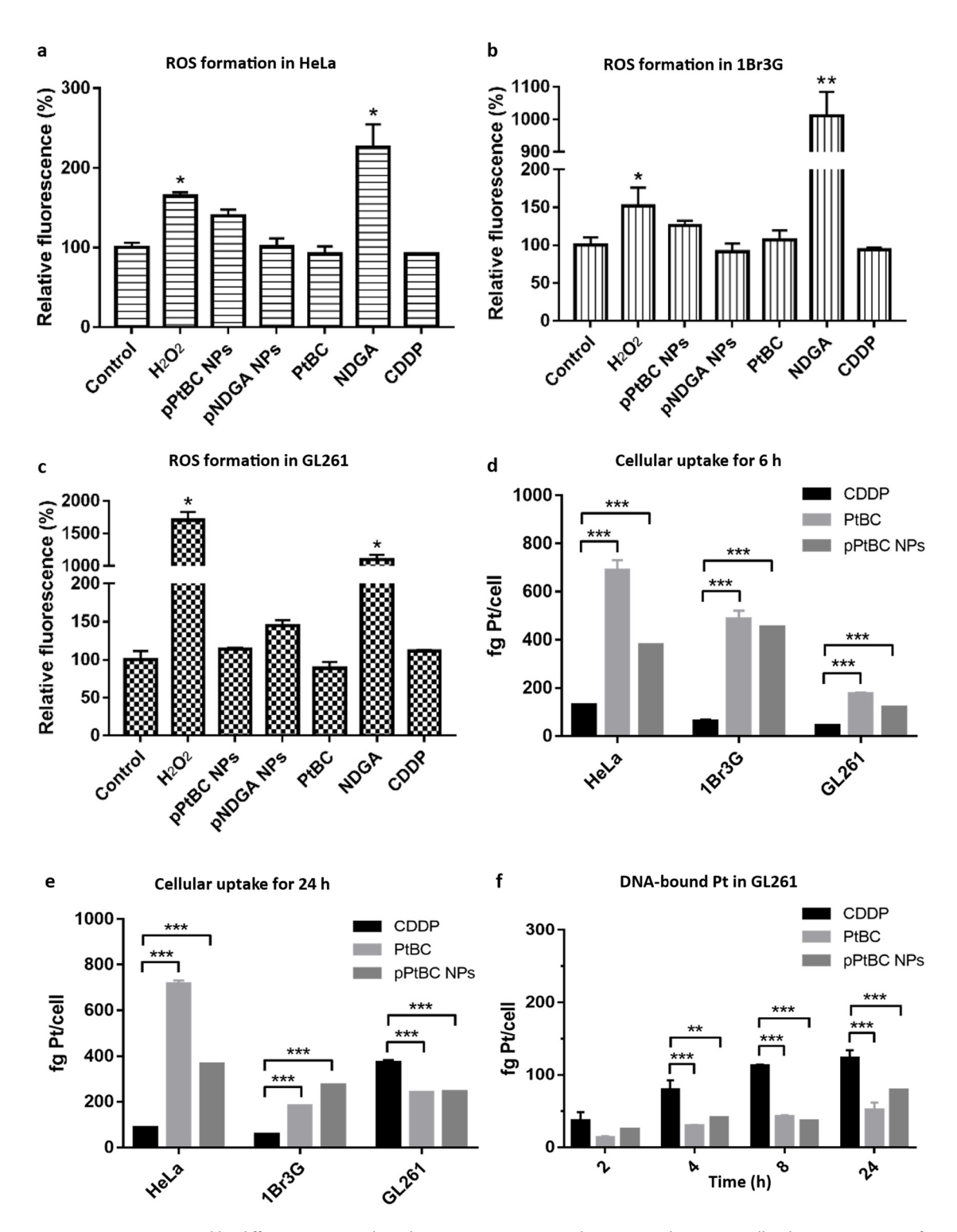
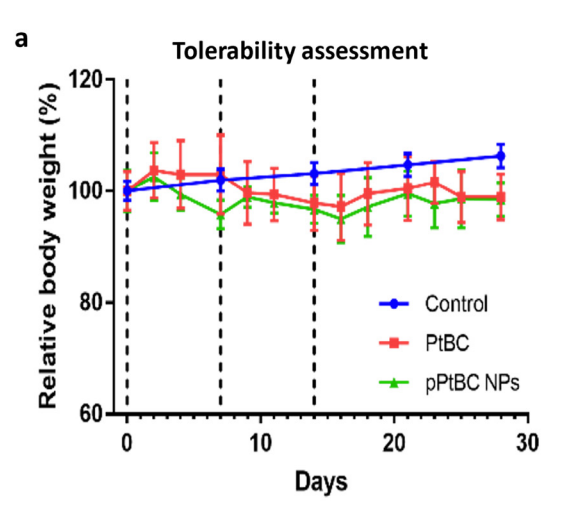


Figure 2: ROS generation triggered by different compounds and pPtBC NPs in (a) HeLa, (b) 1Br3G, and (c) GL261 cells. The concentration of H_2O_2 was 0.1 mM, pNDGA NPs at 0.2 mM, and other agents at their corresponding IC_{50} s. Cellular uptake of CDDP, PtBC, and pPtBC NPs in HeLa, 1Br3G, and GL261 cells for (d) 6 h and (e) 24 h. All drugs were incubated at a concentration of 100 μ M referred to Pt. (f) DNA-bound Pt after exposure to CDDP, PtBC, and pPtBC NPs for 24 h at a concentration of 100 μ M referred to Pt. Each value is represented as mean ± SE of three independent experiments. *stands for p < 0.05, ** for p < 0.001, *** for p < 0.0001.



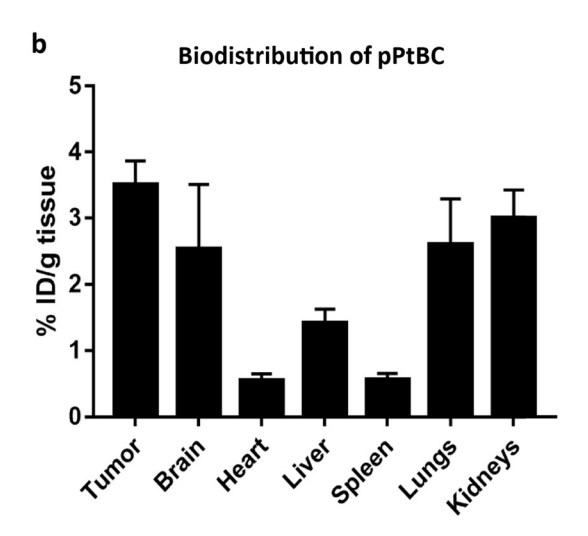


Figure 3: (a) Mice tolerability assessment of mice for PtBC and pPtBC NPs over 4 weeks. Both drugs were administered in incremental doses of 0.9, 1.2–1.5 mg Pt/kg body weight *via* intranasal weekly, n = 3. The control group, comprising n = 360, had data sourced from Jackson Laboratory (https://www.jax.org/jax-mice-and-services/strain-data-sheet-pages/body-weight-chart-000664). (b) Biodistribution of pPtBC NPs in mice bearing GL261 tumors 1 h after administration. Mice were intranasally administered with pPtBC NPs at a dose of 1.5 mg Pt/kg and sacrificed 1 h post-administration. Dashed lines stand for administration days. Each value is represented as mean \pm SE, n = 3.

3.6.1 Safety and tolerability

PtBC and pPtBC NPs were assessed in a dose-escalation experiment using wild-type (wt) C57BL/6 J mice. Increasing doses (0.9, 1.2, and 1.5 mg Pt/kg body weight) were administered over 3 consecutive weeks [57]. Body weight, water/ food consumption, and mouse behavior were evaluated three times over 4 weeks, overlaying with the normal body weight progression of C57BL/6 J mice (control). As shown in Figure 3a, the body weights of all treatment groups remained stable as the control group till the end of the study, indicating an absence of evident systemic toxicity. Notably, no treatment-related adverse effects such as mortality, body weight loss, food consumption, or other clinical signs of mucosa damage were observed for all mice during the study relative to control animals. Even at the highest dosage of 1.5 mg Pt/kg body weight, all mice maintained good health status during the study.

3.6.2 Biodistribution

To assess the accumulation in tumors, these studies were done on mice bearing orthotopic GB tumors with an average size of $24.96 \pm 2.7 \text{ mm}^3$ and a body weight of $22.7 \pm 0.2 \text{ g}$, at the highest dose of 1.5 mg Pt/kg, as part of the tolerability assessment. As depicted in Figure 3b, 1 h post-intranasal administration, Pt predominantly accumulated in the GB tumor, followed by the kidneys, lungs, and brain. Minimal accumulation was observed in the liver, spleen,

and heart. Pt retention in the tumor reached the highest level at 3.51 \pm 0.36% ID/g, while in the brain, lungs, and kidneys, it measured 2.53 \pm 0.98%, 2.6 \pm 0.69, and 3.0 \pm 0.43% ID/g, respectively. No statistically significant differences were observed in Pt retention between the tumor and the organs. However, Pt accumulation in the tumor significantly surpassed that in the heart, liver, and spleen. When considering the tumor and brain collectively, Pt accumulation in the central nervous system was higher than in other organs.

4 Conclusions

A new family of bioinspired platinum-based nanoparticles has been successfully synthesized and characterized. At 72 h, the toxicity of the nanoparticles is close to that of the monomeric unit (in the case of HeLa and 1Br3G even improved), and in both cases, similar or even better than the gold standard cisplatin drug. Additional advantages of the bioinspired nanostructuration are: (I) our NPs present a much better cellular uptake over short periods of time, allowing for a better drug accumulation over the typical short windows before renal clearance; (II) NPs exhibit an effective long-lasting release: even its improved cellular uptake, the cytotoxicity at 24 h and the DNA-bound Pt is lower for NPs while slightly better at 72 h; (III) our NPs favour intranasal administration, overcoming the low drug concentration that cisplatin-based drugs have always struggled to achieve; and

(IV) our system exhibits activation and release patterns (pH and GSH sensitivity), classically employed to avoid undesired side effects because of off-target drug activation.

An additional advantage of our approach is the expected reduction of undesired side effects, thanks to (I) the use of an unactive Pt(IV) precursor that is reduced intracellularly to the active Pt(II) (a widely reported phenomena with several Pt(IV) complexes exhibiting this phenomena [58-60] and the corresponding mechanisms) [61–64]; and (II) the relevance of pH and GSH-sensitive pPtBC NPs to effectively activate the release of the platinum cargo at the desired specific target, thanks to the hydrolysis potential of amide bonds and reduction susceptibility of Pt(IV) complexes in the presence of a reductive environment breaking any axially bonded substitution and realizing Pt(II) cargo. [65-67] Finally, in vivo experiments demonstrated excellent biocompatibility and tolerability of the nanoparticles as a distinctive pharmacokinetic pathway associated intranasal delivery different from other systemic routes.

Acknowledgments: We would like to acknowledge the "Cell Cultures, Antibody Production and Cytometry Services" of the Institut de Biotecnologia i de Biomedicina (IBB) associated with the Universitat Autònoma de Barcelona (UAB) for their collaboration in the cell culture and cytometric assays.

Funding information: This work was supported by grants PID2021-127983OB-C21 and PID2021-127983OB-C22 funded by MCIN/AEI/10.13039/501100011033/and ERDF. A way of making Europe. F. N. acknowledges support by grant CNS2022-136106 funded by MICIU/AEI/10.13039/501100011033 and by European Union NextGeneration EU/PRTR. The ICN2 is funded by the CERCA program/Generalitat de Catalunya and supported by the Severo Ochoa Centres of Excellence program, grant CEX2021-001214-S, funded by MCIN/AEI/10.13039.501100011033.

Author contributions: All authors have accepted responsibility for the entire content of this manuscript and approved its submission. R.G and P.A.: methodology, investigation, data curation, formal analysis, validation, visualization, writing – original draft, review and editing. X. Mao: methodology, investigation, data curation, formal analysis. J. Mancebo: synthesis and data curation, formal analysis, visualization, editing. D. Montpeyo: cell culture. F. Novio: conceptualization, methodology, supervision, Writing - review and editing. Julia Lorenzo: Conceptualization, Resources, Funding acquisition, Writing – review & editing. D. Ruiz-Molina: Resources, Supervision, Project administration, Funding acquisition, Writing - review and editing.

Conflict of interest: The authors state no conflict of interest.

Data availability statement: The datasets generated and/ or analysed during the current study are available from the corresponding author on reasonable request.

References

- Zhang C, Xu C, Gao X, Yao Q. Platinum-based drugs for cancer therapy and anti-tumor strategies. Theranostics. 2022;12:2115-32.
- Zhang J, Li X, Han X, Liu R, Fang J. Targeting the thioredoxin system for cancer therapy. Trends Pharmacol Sci. 2017;38:794-808.
- [3] Bian M. Fan R. Zhao S. Liu W. Targeting the thioredoxin system as a strategy for cancer therapy. J Med Chem. 2019;62:7309-21.
- Park GY, Wilson JJ, Song Y, Lippard SJ. Phenanthriplatin, a mono-[4] functional DNA-binding platinum anticancer drug candidate with unusual potency and cellular activity profile. Proc Natl Acad Sci USA. 2012;109:11987-92.
- [5] Florea AM, Büsselberg D. Cisplatin as an anti-tumor drug: Cellular mechanisms of activity, drug resistance and induced side effects. Cancers. 2011;3(1):1351-71.
- Ohmichi M, Hayakawa J, Tasaka K, Kurachi H, Murata Y. Mechanisms of platinum drug resistance. Trends Pharmacol Sci. 2005;26(3):113-6.
- Wang D, Lippard SJ. Cellular processing of platinum anticancer drugs. Nat Rev Drug Discov. 2005;4(4):307-20.
- Corte-Rodríguez M, Espina M, Sierra LM, Blanco E, Ames T, Montes-[8] Bayón M, et al. Quantitative evaluation of cellular uptake, DNA incorporation and adduct formation in cisplatin sensitive and resistant cell lines: Comparison of different Pt-containing drugs. Biochem Pharmacol. 2015;98:69-77.
- Qi L, Luo Q, Zhang Y, Jia F, Zhao Y, Wang F. Advances in toxicological research of the anticancer drug cisplatin. Chem Res Toxicol. 2019;32(8):1469-86.
- [10] Wong E, Giandornenico CM. Current status of platinum-based antitumor drugs. Chem Rev. 1999;99(9):2451-66.
- Wlodarczyk MT, Dragulska SA, Camacho-Vanegas O, Dottino PR, Jarzecki AA, Martignetti JA, et al. Platinum(II) complex-nuclear localization sequence peptide hybrid for overcoming platinum resistance in cancer therapy. ACS Biomater Sci Eng. 2018;4(2):463-7.
- [12] Mjos KD, Orvig C. Metallodrugs in medicinal inorganic chemistry. Chem Rev. 2014;114(8):4540-63.
- [13] Gibson D. Multi-action Pt(IV) anticancer agents; do we understand how they work? J Inorg Biochem. 2019;191:77-84.
- Wang Z, Xu Z, Zhu G. A platinum(IV) anticancer prodrug targeting [14] nucleotide excision repair to overcome cisplatin resistance. Angew Chem Int Ed. 2016;55(50):15564-8.
- Chen S, Yao H, Zhou Q, Tse MK, Gunawan YF, Zhu G. Stability, reduction, and cytotoxicity of platinum(IV) anticancer prodrugs bearing carbamate axial ligands: Comparison with their carboxylate analogues. Inorg Chem. 2020;59(16):11676-7.
- [16] Wong DY, Yeo CH, Ang WH. Immuno-chemotherapeutic platinum (IV) prodrugs of cisplatin as multimodal anticancer agents. Angew Chem Int Ed. 2014;53(26):6752-56.
- [17] Gibson D. Platinum (IV) anticancer agents; are we en route to the holy grail or to a dead end? | Inorg Biochem. 2021;217:111353-63.
- Dhami NK, Pandey RS, Jain UK, Chandra R, Madan J. Non-aggregated protamine-coated poly(lactide-co-glycolide) nanoparticles of

- cisplatin crossed blood-brain barrier, enhanced drug delivery and improved therapeutic index in glioblastoma cells: In vitro studies. J Microencapsul. 2014;31(7):685-93.
- [19] Depciuch J, Miszczyk J, Maximenko A, Zielinski PM, Rawojć K, Panek A, et al. Gold nanopeanuts as prospective support for cisplatin in glioblastoma nano-chemo-radiotherapy. Int J Mol Sci.
- [20] Wu H, Cabral H, Toh K, Mi P, Chen YC, Matsumoto Y, et al. Polymeric micelles loaded with platinum anticancer drugs target preangiogenic micrometastatic niches associated with inflammation. J Controlled Release. 2014;189:1-10.
- [21] Kesavan A, Ilaiyaraja P, Beaula WS, Kumari VV, Lal JS, Arunkumar C, et al. Tumor targeting using polyamidoamine dendrimer-cisplatin nanoparticles functionalized with diglycolamic acid and herceptin. Eur | Pharm Biopharm. 2015;96:255-63.
- [22] Barth RF, Wu G, Meisen WH, Nakkula RJ, Yang W, Huo T, et al. Design, synthesis, and evaluation of cisplatin-containing EGFR targeting bioconjugates as potential therapeutic agents for brain tumors. OncoTargets Ther. 2016;9:2769-81.
- [23] Thanasupawat T, Bergen H, Hombach-Klonisch S, Krcek J, Ghavami S, Del Bigio MR, et al. Platinum (IV) coiled coil nanotubes selectively kill human glioblastoma cells. Nanomedicine. 2015;11(4):913-25.
- [24] Mathew EN, Berry BC, Yang HW, Carroll RS, Johnson MD. Delivering therapeutics to glioblastoma: Overcoming biological constraints. Int J Mol Sci. 2022;23(3):1711-24.
- [25] Harder BG, Blomquist MR, Wang J, Kim AJ, Woodworth GF, Winkles JA, et al. Developments in blood-brain barrier penetrance and drug repurposing for improved treatment of glioblastoma. Front Oncol. 2018;8:462.
- [26] Zhang Y, Fu X, Jia J, Wikerholmen T, Xi K, Kong Y, et al. Glioblastoma therapy using codelivery of cisplatin and glutathione peroxidase targeting siRNA from iron oxide nanoparticles. ACS Appl Mater Interfaces. 2020;12(39):43408-21.
- [27] Saraiva C, Praça C, Ferreira R, Santos T, Ferreira L, Bernardino L. Nanoparticle-mediated brain drug delivery: Overcoming bloodbrain barrier to treat neurodegenerative diseases. J Controlled Release. 2016:235:34-47.
- [28] Hersh DS, Wadaikar AS, Roberts NB, Perez JG, Connolly NP, Frenkel V, et al. Evolving drug delivery strategies to overcome the blood brain barrier. Curr Pharm Des. 2016;22(9):1177-93.
- [29] Liang S, Zhou Q, Wang M, Zhu Y, Wu Q, Yang X. Water-soluble I-cysteine-coated FePt nanoparticles as dual MRI/CT imaging contrast agent for glioma. Int J Nanomed. 2015;10:2325-33.
- [30] Sun H, Chen X, Chen D, Dong M, Fu X, Li Q, et al. Influences of surface coatings and components of FePt nanoparticles on the suppression of glioma cell proliferation. Int J Nanomed. 2012;7:3295-307.
- [31] Alfonso-Triguero P, Lorenzo J, Candiota AP, Arús C, Ruiz-Molina D, Novio F. Platinum-based nanoformulations for glioblastoma treatment: the resurgence of platinum drugs? Nanomaterials
- [32] Ruiz-Molina D, Mao X, Alfonso-Triguero P, Lorenzo J, Bruna J, Yuste VJ, et al. Advances in preclinical/clinical glioblastoma treatment: Can nanoparticles be of help? Cancers. 2022;14(19):4960-85.
- [33] Bigaj-Józefowska MJ, Coy E, Załęski K, Zalewski T, Grabowska M, Jaskot K, et al. Biomimetic theranostic nanoparticles for effective anticancer therapy and MRI imaging. J Photochem Photobiol B. 2023:249:112813.

- [34] Mrówczyński R, Grześkowiak BF. Biomimetic catechol-based nanomaterials for combined anticancer therapies. Nanoeng Biomater. 2021;1:145-80.
- [35] Liu L, Ye Q, Lu M, Lo YC, Hsu YH, Wei MC, et al. A new approach to reduce toxicities and to improve bioavailabilities of platinum-containing anti-cancer nanodrugs. Sci Rep. 2015;5(1):10881-92.
- Liebscher J. Chemistry of polydopamine-scope, variation, and limitation. Eur I Org Chem. 2019:2019(31-32):4976-94.
- [37] Alfieri ML, Weil T, Ng DY, Ball V. Polydopamine at biological interfaces. Adv Colloid Interface Sci. 2022;305:102689.
- [38] Alfieri ML, Panzella L, Napolitano A. Multifunctional coatings hinging on the catechol/amine interplay. Eur J Org Chem.
- [39] Mao X, Wu S, Calero-Pérez P, Candiota AP, Alfonso P, Bruna J, et al. Synthesis and validation of a bioinspired catechol-functionalized pt (IV) prodrug for preclinical intranasal glioblastoma treatment. Cancers. 2022;14(2):410-25.
- [40] Mao X, Calero-Pérez P, Montpeyó D, Bruna J, Yuste VJ, Candiota AP, et al. Intranasal administration of catechol-based pt(IV) coordination polymer nanoparticles for glioblastoma therapy. Nanomaterials. 2022;12(7):1221-43.
- [41] Labet M, Thielemans W. Synthesis of polycaprolactone: A review. Chem Soc Rev. 2009;38(12):3484-504.
- [42] Wei Q, Zhang F, Li J, Li B, Zhao C. Oxidant-induced dopamine polymerization for multifunctional coatings. Polym Chem. 2010;1(9):1430-3.
- Lee SM, O'Halloran TV, Nguyen ST. Polymer-caged nanobins for [43] synergistic cisplatin-doxorubicin combination chemotherapy. | Am Chem Soc. 2010;132(48):17130-8.
- [44] Lushchak VI. Glutathione homeostasis and functions: Potential targets for medical interventions. J Amino Acids. 2012;2012:1-26.
- [45] Liu Z, Wang M, Wang H, Fang L, Gou S. Platinum-based modification of styrylbenzylsulfones as multifunctional antitumor agents: Targeting the RAS/RAF pathway, enhancing antitumor activity, and overcoming multidrug resistance. J Med Chem. 2019;63(1):186-204.
- [46] Mao X, Si J, Huang Q, Sun X, Zhang Q, Shen Y, et al. Self-assembling doxorubicin prodrug forming nanoparticles and effectively reversing drug resistance In vitro and In vivo. Adv Healthcare Mater. 2016:5(19):2517-27.
- [47] Mahmoudi M, Laurent S, Shokrgozar MA, Hosseinkhani M. Toxicity evaluations of superparamagnetic iron oxide nanoparticles: Cell 'vision' versus physicochemical properties of nanoparticles. ACS Nano. 2011;5(9):7263-76.
- [48] Kumar N, Goel N. Phenolic acids: Natural versatile molecules with promising therapeutic applications. Biotechnol Rep. 2019;24:e00370.
- [49] Forooshani PK, Meng H, Lee BP. Catechol redox reaction: Reactive oxygen species generation, regulation, and biomedical applications. ACS Symp Ser. 2017;1:179-96.
- [50] Eruslanov E, Kusmartsev S. Identification of ROS using oxidized DCFDA and flow-cytometry. Methods Mol Biol. 2010;594:57-72.
- Kreuter J. Drug delivery to the central nervous system by polymeric nanoparticles: What do we know? Adv Drug Deliv Rev. 2014;71:2-14.
- Yonezawa A, Masuda S, Yokoo S, Katsura T, Inui KI. Cisplatin and [52] oxaliplatin, but not carboplatin and nedaplatin, are substrates for human organic cation transporters (SLC22A1-3 and multidrug and toxin extrusion family). J Pharmacol Exp Ther. 2006;319(2):879-86.
- Howell SB, Safaei R, Larson CA, Sailor MJ. Copper transporters and the cellular pharmacology of the platinum-containing cancer drugs. Mol Pharmacol. 2010;77(6):887-94.

- [54] Tesniere A, Schlemmer F, Boige V, Kepp O, Martins I, Ghiringhelli F, et al. Immunogenic death of colon cancer cells treated with oxaliplatin. Oncogene. 2010;29(4):482–91.
- [55] Chapman EG, DeRose VJ. Enzymatic processing of platinated RNAs. J Am Chem Soc. 2010;132(6):1946–52.
- [56] Bose RN, Maurmann L, Mishur RJ, Yasui L, Gupta S, Grayburn WS, et al. Non-DNA-binding platinum anticancer agents: Cytotoxic activities of platinum-phosphato complexes towards human ovarian cancer cells. Proc Natl Acad Sci USA. 2008;105(47):18314–9.
- [57] Shader RI. Safety versus tolerability. Clin Ther. 2018;40(5):672–3.
- [58] Varbanov H, Valiahdi SM, Legin AA, Jakupec MA, Roller A, Bernhard K, et al. Synthesis and characterization of novel bis(car-boxylato)dichloridobis(ethylamine)platinum(IV) complexes with higher cytotoxicity than cisplatin. Eur J Med Chem. 2011;46(11):5456–64.
- [59] Tolan D, Gandin V, Morrison L, El-Nahas A, Marzano C, Montagner D, et al. Oxidative stress induced by Pt(IV) pro-drugs based on the cisplatin scaffold and indole carboxylic acids in axial position. Sci Rep. 2016;6:29367.
- [60] Mi Q, Shu S, Yang C, Gao C, Zhang X, Luo X, et al. Current status for oral platinum (IV) anticancer drug development. Int J Med Phys Clin Eng Radiat Oncol. 2018;7(2):231–2.

- [61] Wexselblatt E, Gibson D. What do we know about the reduction of Pt(IV) pro-drugs? J Inorg Biochem. 2012;117:220–9.
- [62] Kuang X, Chi D, Li J, Guo C, Yang Y, Zhou S, et al. Disulfide bond-based cascade reduction-responsive Pt(IV) nanoassemblies for improved anti-tumor efficiency and biosafety. Colloids Surf B. 2021;203:111766.
- [63] Matthew DH, Trevor WH. Platinum(IV) antitumour compounds: their bioinorganic chemistry. Coord Chem Rev. 2002;232(1–2):49–67.
- [64] Nagyal L, Kumar A, Sharma R, Yadav R, Chaudhary P, Singh R. Bioinorganic chemistry of platinum(IV) complexes as platforms for anticancer agents. Curr Bioact Compd. 2020;16(7):726–37.
- [65] Liu XM, Zhu ZZ, He XR, Zou YH, Chen Q, Wang XY, et al. NIR light and GSH dual-responsive upconversion nanoparticles loaded with multifunctional platinum (IV) prodrug and RGD peptide for precise cancer therapy. ACS Appl Mater Interfaces. 2024;16(31):40753–66.
- [66] Schmidt C, Babu T, Kostrhunova H, Timm A, Basu U, Ott I, et al. Are Pt (IV) prodrugs that release combretastatin A4 true multi-action prodrugs? | Med Chem. 2021;64(15):11364–78.
- [67] Gabano E, Ravera M, Osella D. Pros and cons of bifunctional platinum (IV) antitumor prodrugs: two are (not always) better than one. Dalton Trans. 2014;43(26):9813–20.